Korean J. Chem. Eng., 39(7), 1796-1804 (2022)
DOI: 10.1007/s11814-022-1112-5

pISSN: 0256-1115
eISSN: 1975-7220

Characteristics of Li_2CO_3 as sintering aid for $Ce_{0.8}Sm_{0.2}O_{2-\delta}$ electrolyte in solid oxide fuel cells

Gwang Seon Park, Su In Mo, Jun Ho Kim, and Jeong Woo Yun†

School of Chemical Engineering, Chonnam National University, Yongbongro 77, Bukgu, Gwangju 61186 Korea
(*Received 15 December 2021 • Revised 21 February 2022 • Accepted 15 March 2022*)

Abstract−Owing to its excellent ionic conductivity, 20 mol% samarium doped ceria ($Ce_{0.8}Sm_{0.2}O_{2-\delta}$, SDC) is considered a promising alternative as an electrolyte in solid oxide fuel cells (SOFCs). SDC electrolytes, however, require high sintering temperatures over 1,600 °C to attain sufficient density to be SOFC electrolytes. To lower the SDC sintering temperature, different amounts of Li_2CO_3 (0-12 mol% of Li) were evaluated as a sintering aid for SDC electrolytes. The SDC electrolyte samples with Li were sintered at 1,400 °C and were compared with SDC electrolytes sintered at 1,600 °C. The SDC electrolyte with 6 mol% of Li sintered at 1,400 °C (Li6SDC1400) was densified to 97.495% of theoretical density (T.D.), which is similar to that achieved by the SDC electrolyte sintered at 1,600 °C (97.433% of T.D.). The improved formation of grain boundary in the Li6SDC1400 sample increased the density of the SDC, resulting in enhancement of ionic conductivity and cell performance. At 800 °C, the maximum power density of the Li6SDC1400 electrolyte sample was 120.15 mW/cm^2.

Keywords: Solid Oxide Fuel Cell, Samarium Doped Ceria, Li_2CO_3 Sintering Aid, Electrolyte, Grain Boundary Conductivity

INTRODUCTION

Solid oxide fuel cells (SOFCs) are promising alternative energy conversion devices because of their low emission and high energy efficiency and fuel flexibility [1-6]. The high operating temperature (800-1,000 °C) of SOFCs enables the direct use of commercial hydrocarbons, such as natural gas, gasoline, and diesel, via internal reforming and/or direct electrochemical oxidation. High operating temperatures, however, confine the selection of sealing and interconnecting materials for SOFC, hindering their use in commercial applications. However, yttria-stabilized zirconia (YSZ, $Y_{0.08}Zr_{0.92}O_2$), widely used as a SOFC electrolyte, does not have sufficient ionic conductivity below 800 °C.

The ceria-based cubic fluorite structured electrolyte has received considerable attention to overcome the limitations of YSZ electrolyte owing to its excellent ionic conductivity [7,8]. Owing to the poor ionic conductivity of pure ceria, aliovalent cations such as Sm^{3+} and Gd^{3+} are introduced as dopants in CeO_2 to create oxygen vacancies for solid-state oxygen transportation. Owing to the similar ionic radii of Sm^{3+} (108 pm with 8 coordination number) and Gd^{3+} (105 pm with 8 coordination number) compared to radius of Ce^{4+} (97 pm with 8 coordination number), samarium doped ceria (SDC), and gadolinium dope ceria (GDC) exhibit excellent ionic conductivity [9]. The formation of oxygen vacancies in SDC is well represented by the Kröger-Vink notation as:

$$Sm_2O_3 \xrightarrow{CeO_2} 2Sm'_{Ce} + 3O_O^X + V_O^{\bullet\bullet} \quad (1)$$

Here, Sm'_{Ce} represents one Ce^{4+} site occupied by Sm^{3+} cation and one oxygen vacancy ($V_O^{\bullet\bullet}$) is formed for every two Sm^{3+} ions incorporated into the ceria lattice. The formation of oxygen vacancies plays a significant role in the O^{2-} ion conduction in the SDC phase.

The ionic conductivity strongly depends on temperature because the movement of oxygen ions is a consequence of the thermally activated hopping mechanism among lattice sites. The ionic conductivity is also affected by sintering conditions, dopant ionic radius and concentration, grain boundary, and grain size [10-13]. Among these factors affecting the ionic conductivity, sintering temperature to achieve the desired density of electrolyte can be the most important factor that determines the cell performance and manufacturing costs. Enhancement of density of the electrolyte directly affects the ionic conductivity, thus improving cell performance. The sintering temperature also determines the grain boundary formation and grain size growth, which significantly affects the electrical property, especially the grain boundary conductivity of the doped ceria [12]. Grain boundaries play a crucial role in determining electrolyte performance as they offer a fast diffusion path for oxygen ions [14-16].

High-temperature sintering is required to achieve the desired density and sufficient ionic conductivity for SOFC electrolytes. The doped-ceria electrolyte such as SDC and GDC requires sintering over 1,600 °C to reach acceptable densification, which is a much higher temperature compared to that used for YSZ electrolyte (~1,400 °C). The sintering process over 1,600 °C leads to interlayer solid-state diffusion between electrolyte and electrode to form by-products that are detrimental for the cell performance while increasing manufacturing costs. To overcome these problems, the sintering temperature needs to be reduced. One of the solutions could be the reduction of the initial particle size to increase the thrust of sintering [17,18]. However, a small pore size among ultra-fine particles produces a high capillary force in the powder compact, causing cracks during

†To whom correspondence should be addressed.
E-mail: jwyun@jnu.ac.kr

drying and firing [19,20]. Another viable solution is to reduce the sintering temperature by using sintering aids. Maheshwari et al. reported that 20 wt% Na_2CO_3 in $Ca_{0.05}Ce_{0.95}O_{2-\delta}$ (CDC) electrolyte as a sintering aid improved the total conductivity 25 times than that of pure CDC electrolyte [21]. Le et al. improved grain boundary conductivity and obtained a relative density of 99.5% upon sintering SDC electrolyte at 898 °C by using Li_2O as a sintering aid [22]. Yoshida and co-workers used Mn_2O_3 and Co_3O_4 as a sintering aid for SDC electrolytes to obtain sufficient density at relatively low sintering temperature and to enhance the grain boundaries [23]. ZnO also proved to be an effective sintering aid for ceria-based electrolytes [24].

In this study, we investigated varying amounts of Li_2CO_3 as a sintering aid to achieve acceptable densification in the SDC electrolyte at reduced sintering temperatures. We studied the ionic conductivity and grain boundary formation as a function of the amount of Li_2CO_3. The electrochemical performance of the SDC electrolyte was also investigated by varying the quantity of Li_2CO_3 and sintering temperature.

EXPERIMENTAL

Li_2CO_3 (99.99%, Aldrich) powder was added to SDC powder (SDC20-M, Fuel cell materials) by varying Li^+ amounts (0, 3, 5, 5.5, 6, 6.5, 7, 9, and 12 mol%) in ethanol and ball-milled for 24 h at room temperature. The slurry was dried at 90 °C and calcined at 600 °C for 2 h. After filtering with 180 μm sieve, the powder was die-pressed uniaxially at 80 bar to form disk-type pellet. The prepared pellets were sintered at 1,400 °C for 5 h. Simultaneously, pure SDC electrolytes were prepared by sintering at 1,600 °C to investigate the effect of Li_2CO_3 sintering aid. The relative densities of the pellet-type samples were measured by the Archimedes method (listed in Table 1).

The structure of the synthesized electrolytes was analyzed with an X-ray diffractometer (XRD, Rigaku, RINT-5200, Japan). The thermal reaction of Li_2CO_3 as a sintering aid was analyzed by thermogravimetric analysis (TGA, Shimadzu, IRPresitge-21, Japan) and differential scanning calorimetry (DSC, Netzsch, DSC 404 F1, Germany). The microstructure was analyzed using a scanning electron microscope (FE-SEM, Hitachi, SU5000, Japan) at Energy Convergence Core Facility in Chonnam National University. The composition of the prepared electrolyte samples was analyzed by X-ray photoelectron spectroscopy (XPS, VG, Multilab2000, UK) and temperature-programmed reduction (TPR, BEL, BEL-CAT, Japan).

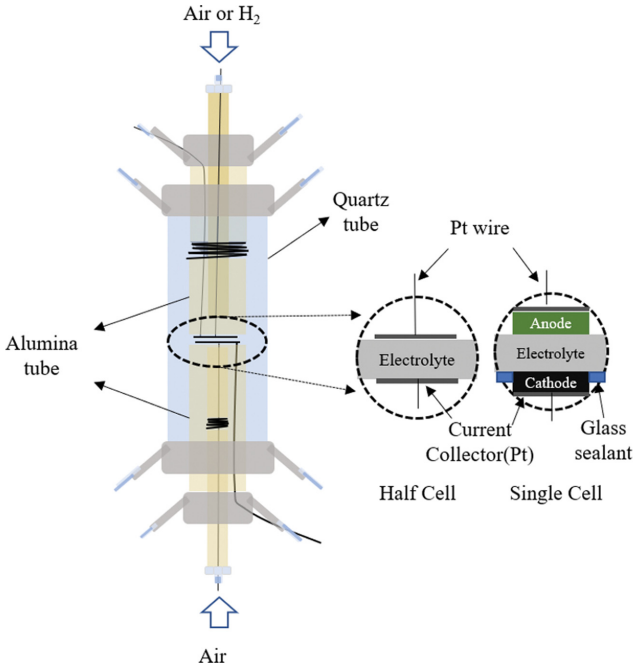

Fig. 1. Schematic of the experimental setup.

To investigate the resistance of the electrolyte, a disk-type half-cell with Pt electrodes was mounted between two double-layer alumina tubes as shown in Fig. 1. A perforated Pt plate and Pt paste were used as the current collectors. Electrochemical property of the cell was analyzed using an impedance analyzer (SP-150, Biologic Science Instrument). The impedance spectra were recorded in the frequency range of 10^{-2}-10^6 Hz with an excitation voltage of 10 mV to ensure a linear response. Impedance analyses were performed at 700-850 °C. Single-cell performance was also measured to investigate the effect of Li_2CO_3. Ni/SDC slurry as an anode material was fabricated by mixing NiO powder and SDC powder in a 7 : 3 weight ratio with the binder, pore former, solvent, and some additives. The

Table 1. Relative density and its standard deviation in electrolytes according to sintering aid content

	Li^+ content (mol %)	Sintering temperature (°C)	Measured density (g/cm^3)	Standard deviation	Relative density (%)
SDC1600	0	1,600	7.006	0.5237	97.433
SDC1400	0	1,400	6.502	1.7989	90.415
Li3SDC1400	3	1,400	6.852	1.0138	95.292
Li5SDC1400	5	1,400	6.956	0.4102	96.726
Li5.5SDC1400	5.5	1,400	6.959	0.3985	96.776
Li6SDC1400	6	1,400	7.011	0.1062	97.495
Li6.5SDC1400	6.5	1,400	6.936	0.4103	96.453
Li7SDC1400	7	1,400	6.904	0.4939	96.008
Li9SDC1400	9	1,400	6.896	0.4103	95.902
Li12SDC1400	**12**	**1,400**	**6.844**	**0.2063**	**95.176**

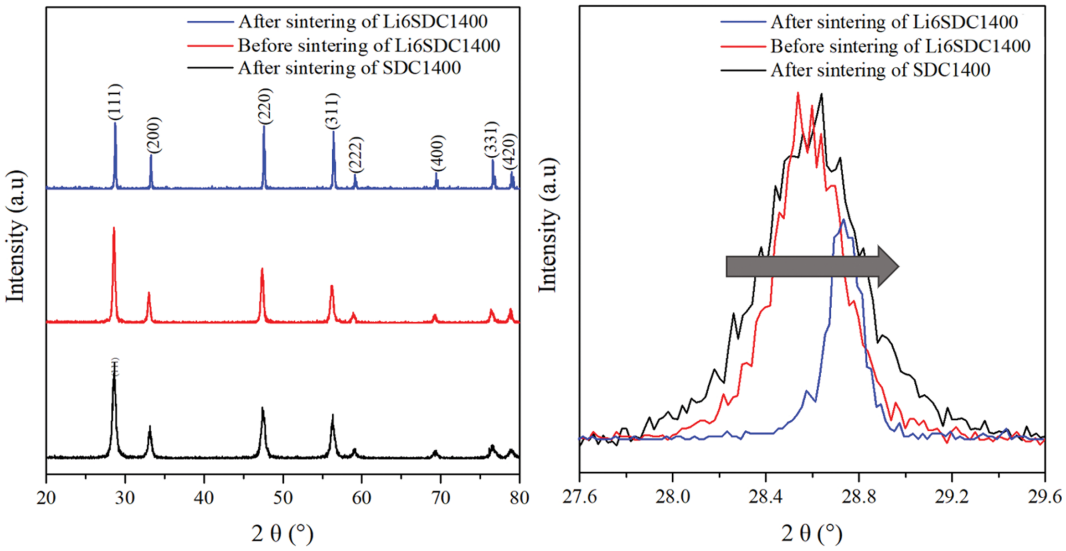

Fig. 2. XRD pattern (a) before and after sintering of Li6SDC1400 and after sintering of SDC1600 and (b) peak magnification of (111) peak.

$La_{0.8}Sr_{0.2}MnO_3$ (LSM, Fuel cell materials) used as the cathode material was also prepared in a slurry state via the same process. The prepared Ni/SDC and LSM slurry were tape-cast on the SDC electrolyte and co-fired for 2 hours at 1,000 °C in air. The anode and cathode areas were 0.95 cm^2.

RESULTS AND DISCUSSION

Fig. 2 shows the XRD pattern of SDC electrolyte with 6 mol% of Li^+ after sintering at 1,400 °C (L060SDC1400) compared to that of pure SDC electrolyte sintered at 1,400 °C (SDC1400). There were no observable peaks of any secondary phase in either of the samples. All peaks of the Li6SDC1400 sample were slightly shifted to a higher angle. The peak shift of the (111) peak is shown in Fig. 2(b). Diffusion of Li into the SDC lattice and Li vaporization may be responsible for the peak shift. In addition, the formation of a small amount of new phase during the sintering process may also contribute to the lattice change. Concerning the lattice shrinkage effect, Li^+ can diffuse into the SDC phase leading to change in the lattice parameter as given by:

$$Li_2CO_3 \xrightarrow{CeO_2} 2Li''_{Ce} + 3V^{\bullet\bullet}_O + O^{\times}_O + CO_2 \quad (2)$$

$$Li_2CO_3 \xrightarrow{Sm_2O_3} 2Li''_{Sm} + 2V^{\bullet\bullet}_O + O^{\times}_O + CO_2 \quad (3)$$

Slightly smaller ionic radii of Li^+ (92 pm with 8 coordinate number) than that of Ce^{4+} (97 pm with 8 coordinate number) and Sm^{3+} (108 pm with 8 coordinate number) can likely substitute into SDC lattice via reaction (2) and (3) with the formation of oxygen vacancies ($V^{\bullet\bullet}_O$). Although Li vaporizes at high sintering temperature, the lattice parameter contraction by Li^+ doping is reflected in the higher-angle shift of the XRD peaks as shown in Fig. 2(b). The oxygen vacancies with two electron holes produced by the reactions (1)-(3) can significantly affect the oxygen ion transfer and improve the ionic conductivity of electrolytes in SOFCs. The low melting temperature of Li_2CO_3 (724 °C) as a sintering aid would promote reactions (2) and (3) while lowering the sintering temperature of the SDC. The phase change of Li_2CO_3 can be inferred from the small exothermic peaks (704 °C) of TGA/DSC results, as shown in Fig. 3.

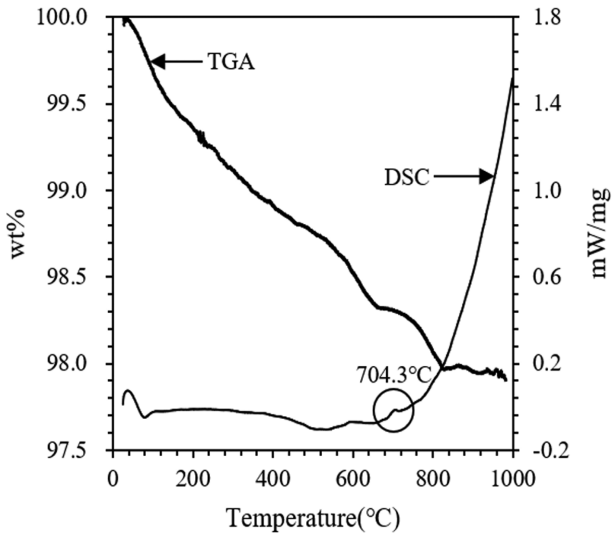

Fig. 3. TGA/DSC results of Li6SDC1400 powder.

Fig. 4 shows the XPS spectra of O1s of (a) Li6SDC1400, (b) SDC1400, and (c) SDC1600 samples. The O1s peak is deconvoluted to a superposition of three sub-peaks, lattice oxygen (O_L), oxygen vacancy (O_V), and absorbed oxygen (O_C) centered at 528.3, 530.1, and 531.6 eV, respectively. The O_L peak is characteristic of O^{2-} of the surface lattice oxygen in the SDC phase. Higher bonding energy O_V peak around 530.1 eV is attributed to oxygen defects in the structure of SDC, related to oxygen vacancies [25]. Peak O_C is related to the surface hydroxyl (OH) group. The concentration of oxygen vacancies was estimated by comparing the relative area ratio of the respective peaks as shown in Table 2. The oxygen vacancies were 15.17%, 7.68%, and 8.66% for Li6SDC1400, (b) SDC1400 and (c) SDC1600, respectively. The oxygen vacancies are formed because of the replacement of Ce^{4+} and/or Sm^{3+} by Li^+ via the dif-

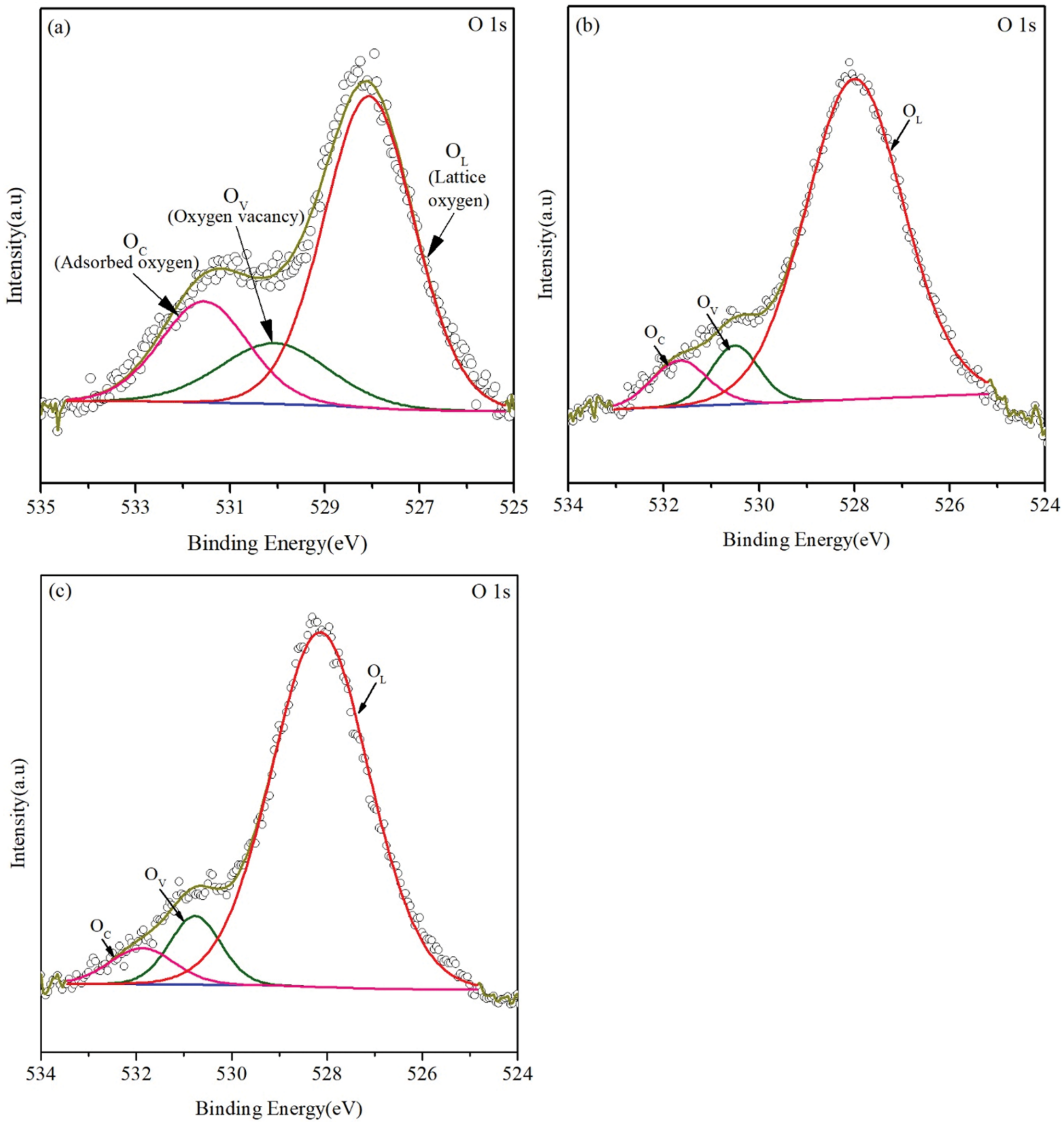

Fig. 4. XPS spectra of O 1s for (a) Li6SDC1400, (b) SDC1400, and (c) SDC1600.

Table 2. Oxygen vacancy estimate from XPS analysis

	Peak binding energy (eV)	Oxygen vacancy at (%)
Li6SDC1400	530.07	15.1699
SDC1400	530.51	7.6819
SDC1600	530.77	8.6589

fusion process through reactions (2) and (3). The peaks shift to slightly lower binding energy upon the addition of Li sintering aid in the Li6SDC1400 sample. The large amounts of oxygen vacancies in the grain boundary space charge layer might be a decisive reason for high grain boundary conductivity, resulting in improved electrolyte conductivity [26-32]. Therefore, the oxygen vacancies formed by the addition of Li_2CO_3 sintering aid would improve the performance of the SDC electrolyte, even though the electrolyte conductivity cannot be solely determined by oxygen vacancies.

Fig. 5(a) shows H_2-TPR results before and after sintering of Li6SDC1400 samples compared to that of pure SDC samples. Two peaks at 596 °C and 653 °C owing to Li_2CO_3 reduction were detected before sintering the samples. After sintering the Li6SDC1400 sample, no additional peaks were detected owing to the Li^+ substitution of Ce^{4+} and/or Sm^{3+} as well as easy evaporation of Li_2CO_3 (melting temperature: 723 °C, boiling temperature: 1,310 °C). The enhanced electronic conductivity from the bulk metallic Li in the electrolyte was detrimental to the SOFC performance because of the thermodynamic potential loss in the SDC electrolyte. The XPS result of Li 1s orbital suggests the elimination of Li metal phase as shown in Fig. 5(b). The Li 1s peaks (54-58 eV) were detected after sintering the Li6SDC1200 sample (sintered at 1,200 °C). No peak was detected after sintering at 1,400 °C, confirming the removal of the metallic Li phase from the SDC electrolyte.

Fig. 6 shows the cross-sectional SEM images of the SDC electrolyte for different amounts of Li_2CO_3 sintering aids (0-12 mol% of Li^+) and sintering temperatures (1,400 °C and 1,600 °C). The density was measured using Archimedes' method. The equation

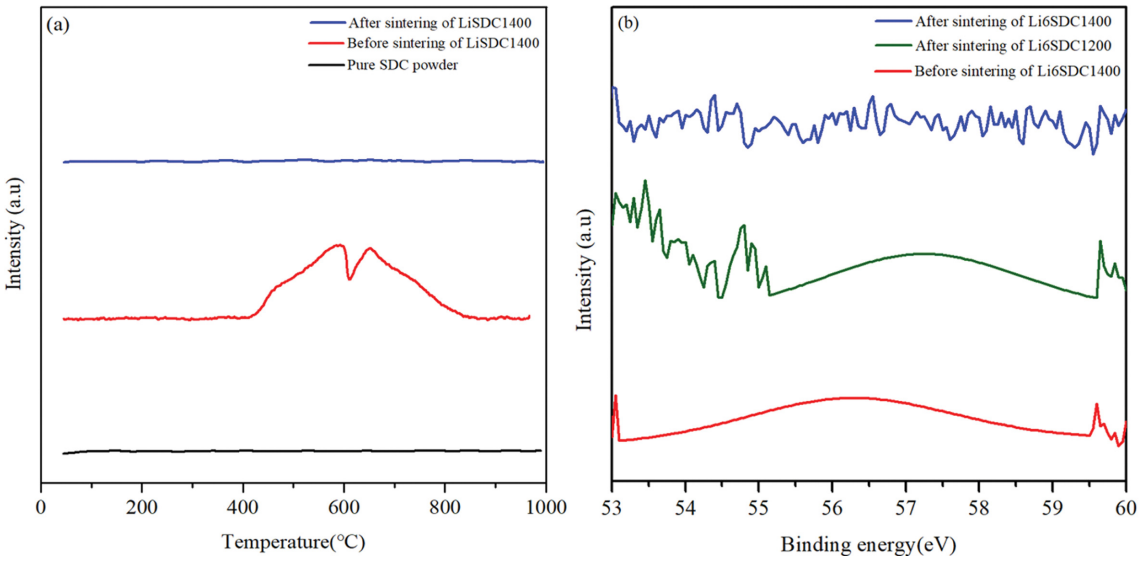

Fig. 5. (a) Before and after sintering H_2-TPR spectra of Li6SDC1400 and pure SDC powder. (b) Pre- and post-sintering XPS analysis of Li6SDC1400 and that of Li6SDC1200 after sintering.

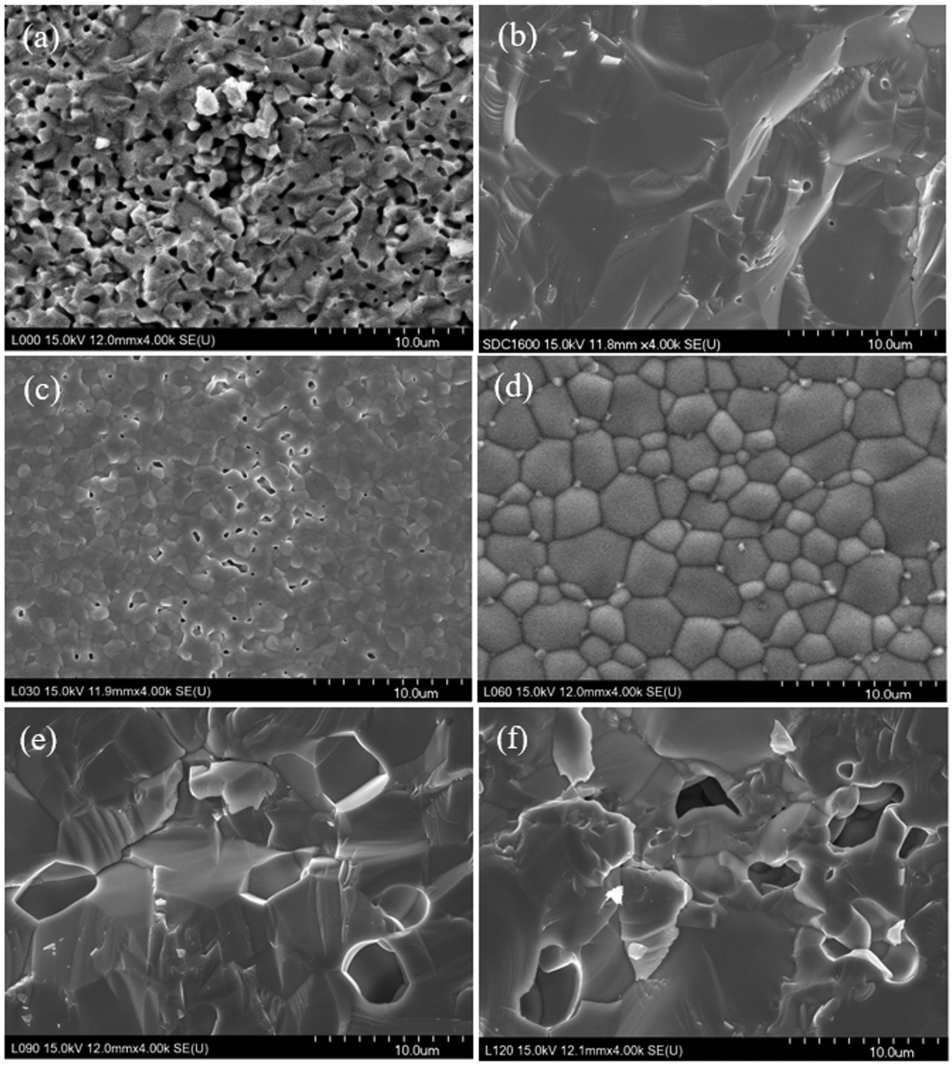

Fig. 6. Cross-sectional SEM images of (a) SDC1400, (b) SDC1600 (c) Li3SDC1400, (d) Li6SDC1400, (e) Li9SDC1400, and (f) Li12SDC1400.

used for measuring the pelletized electrolytes is given as:

$$\rho = \frac{W_1}{W_2 - W_3} \times \rho_1 \quad (4)$$

where W_1 is cell weight in dry air condition, W_2 is cell weight impregnated with distilled water, and W_3 is cell weight in distilled water; ρ_1 is the density of distilled water. The theoretical density of SDC is 7.191 g·cm^{-3} [33]. Because of poor sinterability, the SDC electrolyte without the sintering aid was not sufficiently densified at 1,400 °C, as shown in Fig. 6(a), in contrast to the fully densified sample at 1,600 °C shown in Fig. 6(b). Obtained densities (relative density) of SDC1400 and SDC1600 were 6.502 g·cm^{-3} (90.415%) and 7.006 g·cm °C^3 (97.433%), respectively. The densification of the SDC electrolytes was improved by adding Li_2CO_3 sintering aids. The obtained densities (relative density) of the SDC electrolytes were 6.852 g·cm^{-3} (95.292%), 7.011 g·cm^{-3} (97.495%), 6.896 g·cm^{-3} (95.902%), and 6.844 g·cm^{-3} (95.176%) in (c) Li3SDC1400, (d) Li6SDC1400, (e) Li9SDC1400, and (f) Li12SDC1400, respectively. The results are also listed in Table 1. Small grains were formed in (c) Li3SDC1400 and became obvious in (d) Li6SDC1400 owing to the increased amount of sintering aid. In addition, the Li3SDC1400 showed less densification, exhibiting several micrometer-sized pores, whereas the Li6SDC1400 was more densified without any pores. The relative densities, however, decreased when the amount of sintering aid increased more than 6 mol% of Li^+ because of the formation of pores as shown in Figs. 6(e) and 6(f). A large amount of Li_2CO_3 aid introduced pores during the removal of sintering aids at high temperature, resulting in increased sample porosity. The Li9SDC1400 exhibited tens of micrometer-sized holes and the holes increased further in the Li12SDC1400. The results of relative density with varying mol% of Li^+ are shown in Fig. 7. The relative density of Li6SDC1400 is higher than that of the SDC1600 and the formation of grain boundary is obvious in Li6SDC1400.

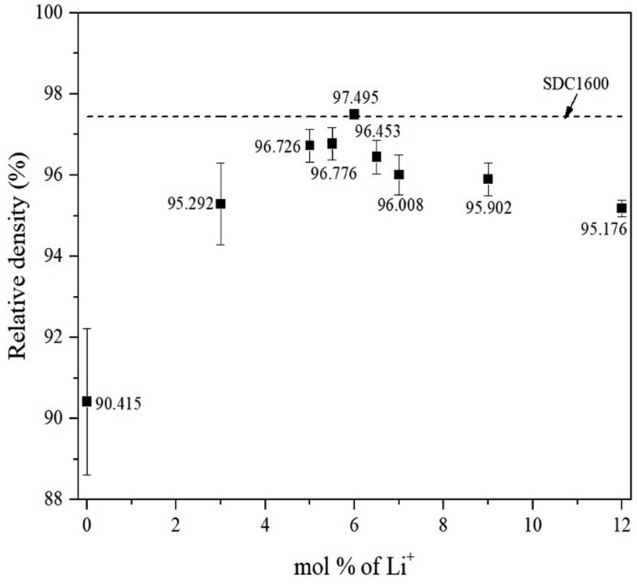

Fig. 7. Relative density variation with Li^+ mol%. The dashed line represents SDC1600.

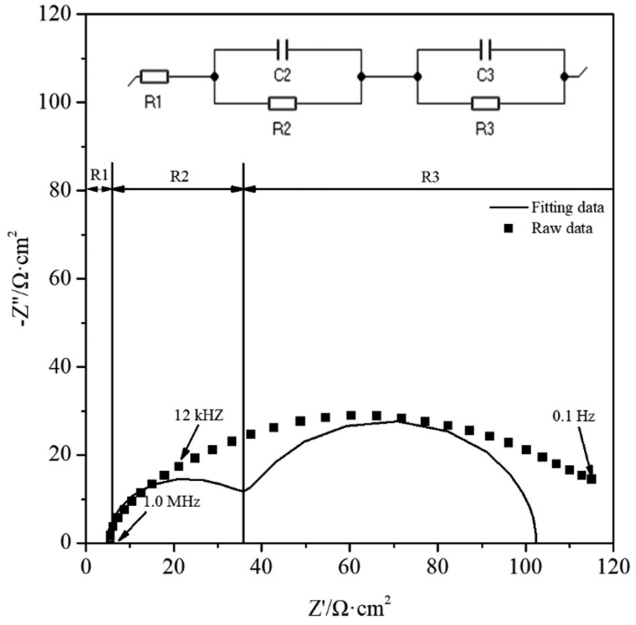

Fig. 8. Equivalent circuit model and Nyquist plot of SDC1600 measured in air at 700 °C.

To investigate electrolyte conductivity, Nyquist curves of electrochemical impedance spectroscopy (EIS) analysis were fitted to an equivalent circuit (top), R1(R2C2)(R3C3), and the SDC1600 sample at 700 °C (bottom), as shown in Fig. 8. The prepared electrolytes were conducted to Pt electrodes in an air atmosphere at 700-850 °C. The circuits were analyzed by a complex nonlinear least square (CNLS) fitting program. Three separate regions were observed in different frequency ranges. R1 corresponds to a high-frequency range and is considered to be the ohmic resistance including ion and electron transport resistance in grains. R2 corresponds to an intermediate frequency arc and involves the movement of ions in grain boundaries. R3 corresponds to a low-frequency arc and is associated with the resistance of the electrolyte/electrode interface. The sum of R2 and R3 is defined as electrode polarization resistance (Rp), which is related to diffusion, adsorption, separation of oxygen molecules, and the migration of oxygen ions to the triple-phase boundaries (TPB) [34,35]. Fig. 9 shows conductivity obtained from the resistance values of the model in Fig. 8. The conductivity increased upon elevating temperature in all samples. The results correspond with the density in Table 1 and Fig. 7. Because of the high densification, the SDC1600 sample showed the highest ohmic conductivity (0.4778 S·cm^{-1}) in contrast to the lowest ohmic conductivity of the SDC1400 sample (0.0681 S·cm^{-1}) at 850 °C. Li6SDC1400 (0.4700 S·cm^{-1}) sample showed similar ohmic conductivity with the SDC1600 sample. Ohmic conductivity, however, decreased in the Li9SDC1400 and Li12SDC1400 samples because of the introduction of pores, as can be seen from Fig. 6. The Li6SDC1400 exhibited the highest grain boundary and interface conductivity of 0.1760 S·cm^{-1} and 0.2717 S·cm^{-1}, respectively, which are higher than that of the SDC1600 with 0.1158 S·cm^{-1} and 0.1427 S·cm^{-1}. The grain boundary and interface conductivity decrease in Li9SDC1400 and Li12SDC1400. Total conductivity at 850 °C attributed to ohmic conductivity, grain boundary con-

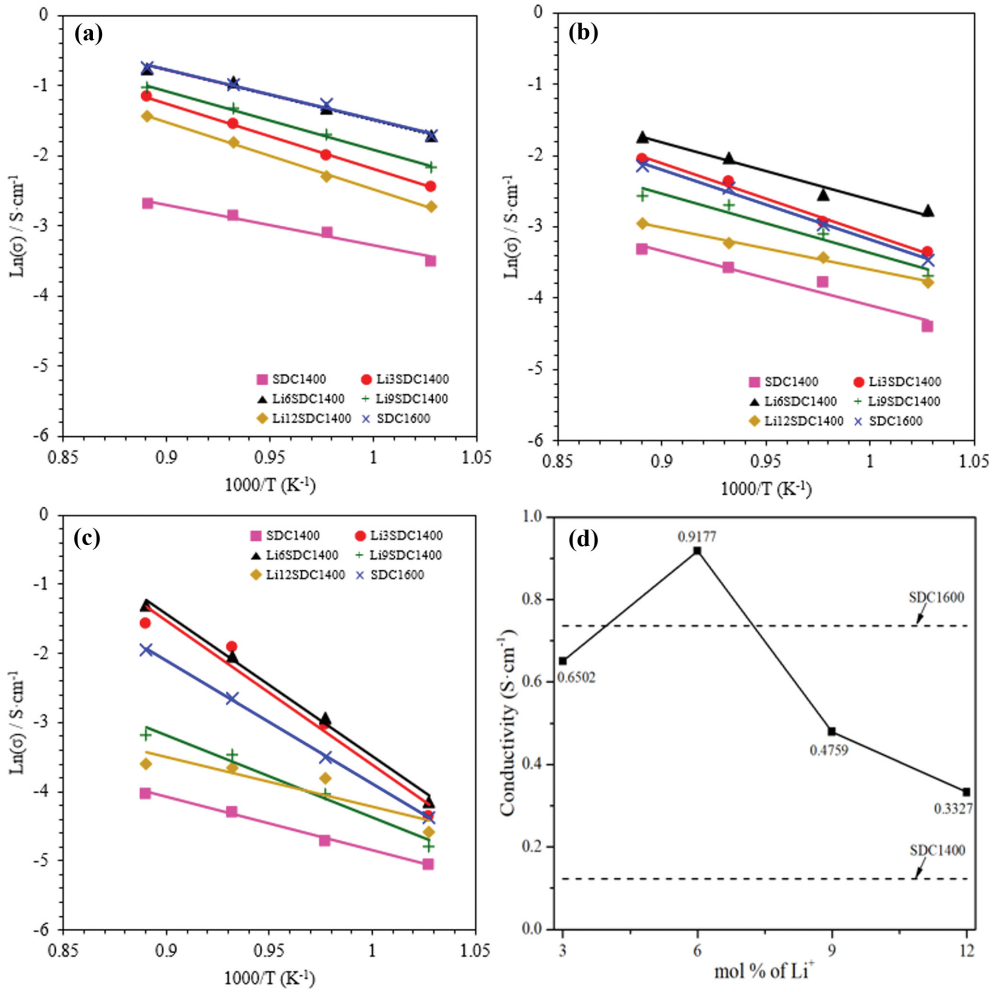

Fig. 9. Arrhenius plots of (a) ohmic conductivity (b) grain boundary conductivity (c) electrode interface conductivity (d) total conductivity.

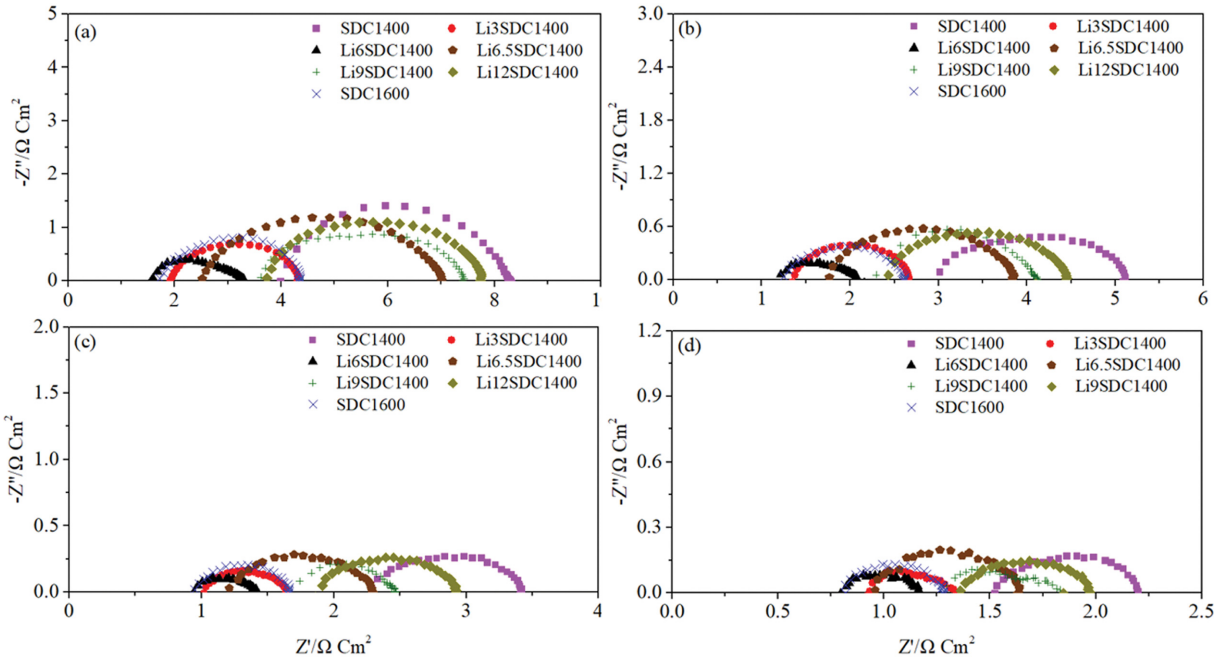

Fig. 10. Nyquist plot of the electrolyte according to the sintering aid content measured at (a) 700 °C, (b) 750 °C, (c) 800 °C, and (d) 850 °C.

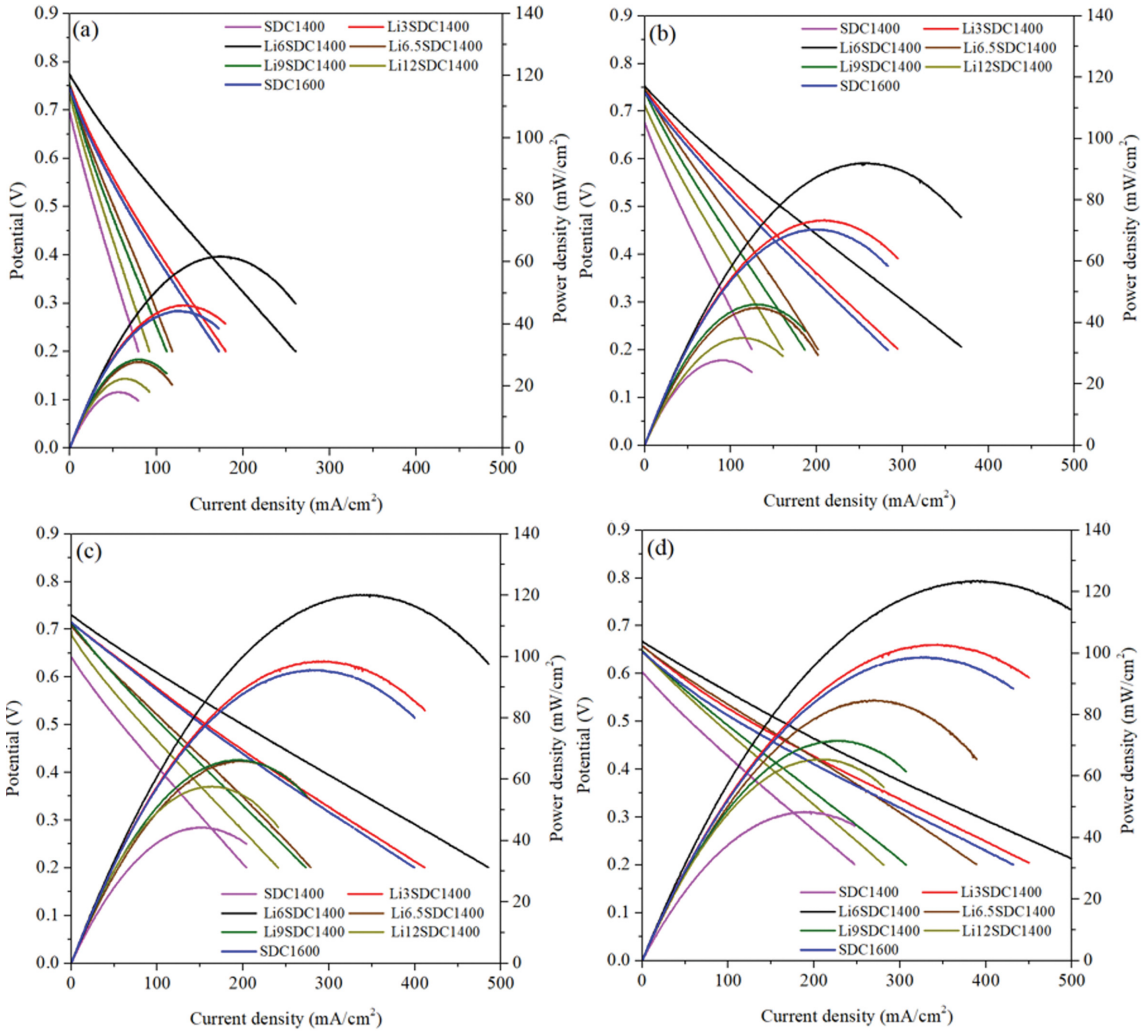

Fig. 11. I-V characteristics of electrolytes measured at (a) 700 °C, (b) 750 °C, (c) 800 °C, and (d) 850 °C.

ductivity, and interface conductivity are plotted in Fig. 9(d). The total conductivities of SDC1400, SDC1600, Li3SDC1400, Li6SDC1400, Li9SDC1400, and Li12SDC1400 were 0.1221 $S \cdot cm^{-1}$, 0.7363 $S \cdot cm^{-1}$, 0.6502 $S \cdot cm^{-1}$, 0.9177 $S \cdot cm^{-1}$, 0.4759 $S \cdot cm^{-1}$, and 0.3327 $S \cdot cm^{-1}$, respectively. The total conductivity increased upon increasing Li^+ concentration till 6 mol% and then decreased for further Li^+ addition. Although both electronic and ionic conductivity contribute to the total conductivity, the oxygen ion vacancy via the reaction (2) and (3) by Li^+ ion substitution increases the total conductivity. The reduction of conductivity observed in the Li9SDC1400 and the Li12SDC1400 is caused by the pore formation as shown in Fig. 6.

To investigate the performance of Li^+ modified SDC electrolyte, button-type single cells with Ni/YSZ anode |Electrolyte| LSM cathode were prepared. Fig. 10 shows the Nyquist plot in the frequency range of 10^{-2}-10^6 Hz for a single cell with different electrolytes at 700-850 °C. Ohmic resistances of the single cells at 700 °C were 4.00, 1.92, 1.57, 3.59, 3.71, and 1.71 $\Omega \cdot cm^2$ in SDC1400, Li3SDC1400, Li6SDC1400, Li9SDC1400, Li12SDC1400, and SDC1600 electrolyte, respectively. At 850 °C, the ohmic resistance was reduced to 1.526, 0.931, 0.799, 1.271, 1.354, and 0.808 $\Omega \cdot cm^2$ in SDC1400, Li3SDC1400, Li6SDC1400, Li9SDC1400, Li12SDC1400, and SDC1600 electrolyte, respectively. The Li6SDC1400 showed the lowest ohmic resistance among the electrolyte samples, even lower than that of the SDC1600. The impedance results agree with the conductivity and sinterability, as shown in Fig. 7 and Fig. 9(d), respectively. The polarization resistances (Rp) show similar behavior with the ohmic resistance, even though the electrodes are the same in all samples.

The I-V characteristics of the single cells as shown in Fig. 11 correspond to the impedance results. The samples of single cells were structurally identical to those in the impedance experiment. Because the SDC has electron conductive material, the open circuit voltage (OCVs) is much lower than that of YSZ electrolyte (1.1-1.2 V). OCVs of the SDC electrolyte and the Li-modified SDC electrolyte were 0.61-0.77 V depending on the electrolytes and decreased with increasing temperature. The maximum power densities at 700 °C were 18.05, 45.98, 61.82, 28.55, 22.34, and 44.14 mW/cm^2 in SDC1400, Li3SDC1400, Li6SDC1400, Li9SDC1400, Li12SDC1400, and SDC1600, respectively. At 800 °C, they increased to 44.31, 98.57, 120.15, 66.3, 57.65, and 95.6 mW/cm^2 in SDC1400, Li3SDC1400, Li6SDC1400, Li9SDC1400, Li12SDC1400. and

SDC1600, respectively. For all samples, the maximum power density did not increase much at 850 °C. The Li6SDC showed the highest cell performance at all temperatures owing to the highest electrical conductivity and excellent sinterability. The appropriate amounts of Li^+ ion in the SDC electrolyte would contribute to the formation of grains and grain boundaries, which might improve the sinterability and the conductivity of the sample. However, the poor sinterability and the low electrical conductivity exhibited in the Li9SDC1400 and the Li12SDC1400 is caused by excessive liquid phase of Li^+ leading to the local over-sintering and pore formation.

CONCLUSIONS

The structural characteristics and electrical performance of the SDC electrolyte and the Li-modified SDC electrolyte were studied for varying amounts of Li^+ ions from 0 to 12 mol%. Li_2CO_3 sintering aid in the SDC electrolyte increased oxygen vacancies by aliovalent substitution of Li^+ for Sm^{3+} and/or Ce^{4+}. The densification of the SDC electrolytes was improved by adding Li_2CO_3 sintering aids. The SDC1400 electrolyte (without the sintering aid) was not sufficiently densified with only 90.415% of relative density. The density of the Li6SDC1400 electrolyte (with 6 mol% of Li^+) increased to 97.495%, which was higher than that of the SDC1600 electrolyte. A large amount of Li_2CO_3 aid (more than 6 mol% of Li^+) led to local over-sintering and introduced pores during the removal of sintering aid. The conductivity results were corroborated with the relative densities of the samples. The electrical conductivity of the Li6SDC1400 electrolyte was 0.4700 $S \cdot cm^{-1}$, which was similar to that of the SDC1600 electrolyte (0.4778 $S \cdot cm^{-1}$). EIS results and I-V characteristics affirmed the conductivity and the sinterability of the samples. The Li6SDC1400 showed the lowest ohmic resistance and the highest cell performance among the electrolyte samples at all temperatures. Our study suggests that Li_2CO_3 can be an effective sintering aid in the SDC electrolyte. In addition, the SDC electrolyte performance can be maximized by optimizing the amount of Li^+ ions and controlling the grain and grain boundary formation.

ACKNOWLEDGEMENTS

This work was supported by the innovation Lab support program for material, parts, equipment (20012555, Commercialization of nanocarbon composites materials in electric and electronic display and energy industries) funded by the Ministry of Trade, Industry & Energy (MOTIE, Korea). This research was supported by Basic Science Research Capacity Enhancement Project through the Korea Basic Science Institute (National Research Facilities and Equipment Center) grant funded by the Ministry of Education.

REFERENCES

1. J. M. Lee and J. W. Yun, *Ceram. Int.*, **42**, 8698 (2016).
2. Z. Zhan, Y. Lin, M. Pillai, I. Kim and S. A. Barnett, *J. Power Sources*, **161**, 460 (2006).
3. R. M. Ormerod, *Chem. Soc. Rev.*, **32**, 17 (2003).
4. D. J. Brett, A. Alan, N. P. Brandon and S. J. Skinner, *Chem. Soc. Rev.*, **37**, 1568 (2008).
5. D. H. Jo, J. H. Chun, K. T. Park, J. W. Hwang, J. Y. Lee, H. W. Jung and S. H. Kim, *Korean J. Chem. Eng.*, **28**, 1844 (2011).
6. J. H. Kim, Y. M. Park, T. Kim and H. Kim, *Korean J. Chem.* Eng., **29**, 349 (2012).
7. M. Chen, H. Zhang, L. Fan, C. Wang and B. Zhu, *Int. J. Hydrogen Energy*, **39**, 12309 (2014).
8. M. Zinkevich, D. Djurovic and F. Aldinger, *Solid State Ionics*, **177**, 989 (2006).
9. T. Zhu, Y. Lin, Z. Yang, D. Su, S. Ma, M. Han and F. Chen, *J. Power Sources*, **261**, 255 (2014).
10. X. Wang, Y. Ma, R. Raza, M. Muhammed and B. Zhu, *Electrochem. Commun.*, **10**, 1617 (2008).
11. B. Singh, A. Bhardwaj, S. K. Gautam, D. Kumar, O. Parkash, I. H. Kim and S. J. Song, *J. Power Sources*, **345**, 176 (2017).
12. G. Zhang, W. Li, W. Huang, Z. Cao, K. Shao, F. Li, C. Tang, C. Li, C. He, Q. Zhang and L. Fan, *J. Power Sources*, **386**, 56 (2018).
13. I. Khan, P. K. Tiwari and S. Basu, *Electrochim. Acta*, **294**, 1 (2019).
14. X. Zhang, C. Deces-Petit, S. Yick, M. Robertson, O. Kesler, R. Maric and D. Ghosh, *J. Power Sources*, **162**, 480 (2006).
15. L. Fan, C. Wang, M. Chen and B. Zhu, *J. Power Sources*, **234**, 154 (2013).
16. B. Zhu, S. Li and B. E. Mellander, *Electrochem. Commun.*, **10**, 302 (2008).
17. P. L. Chen and I. W. Chen, *J. Am. Ceram. Soc.*, **79**, 3129 (1996).
18. P. L. Chen and I. W. Chen, *J. Am. Ceram. Soc.*, **80**, 637 (1997).
19. Z. Tianshu, P. Hing, H. Huang and J. Kilner, *J. Mater. Process Tech.*, **113**, 463 (2001).
20. C. Herring, *J. Appl. Phys.*, **21**, 301 (1950).
21. J. Wang, X. Chen, S. Xie, L. Chen, Y. Wang, J. Meng and D. Zhou, *J. Power Sources*, **428**, 105 (2019).
22. S. Le, S. Zhu, X. Zhu and K. Sun, *J. Power Sources*, **222**, 367 (2013).
23. H. Yoshida and T. Inagaki, *J. Alloy. Compd.*, **408**, 632 (2006).
24. L. A. Villas-Boas. F. M. l. Figueiredo, D. P. F. de Souza and F. B. M. Marques, *Solid State Ionics*, **262**, 522 (2014).
25. T. Wei, L. Jia, J. Luo, B. Chi, J. Pu and J. Li, *Appl. Surf. Sci.*, **506**, 144699 (2020).
26. X. Guo, *Solid State Ionics*, **81**, 235 (1995).
27. X. Guo, *Solid State Ionics*, **96**, 247 (1997).
28. X. Guo, *Comp. Mater. Sci.*, **20**, 168 (2001).
29. X. Guo, W. Sigle, J. Fleig and J. Maier, *Solid State Ionics*, **154**, 555 (2002).
30. X. Guo and Z. Zhang, *Acta Mater.*, **51**, 2539 (2003).
31. J. C. M'Peko and M. F. de Souza, *Appl. Phys. Lett.*, **83**, 737 (2003).
32. X. Guo and R. Waser, *Prog. Mater. Sci.*, **51**, 151 (2006).
33. G. Ruifeng and M. Zongqiang, *J. Rare Earth*, **25**, 364 (2007).
34. B. S. Prakash, S. S. Kumar and S. R. Aruna, *B. Mater. Sci.*, **40**, 441 (2017).
35. X. Nie, Y. Chen, N. Mushtaq, S. Rauf, B. Wang, W. Dong, X. Wang, H. Wang and B. Zhu, *Nanoscale Res. Lett.*, **14**, 1 (2019).